NJC

Accepted Manuscript

This is an *Accepted Manuscript*, which has been through the Royal Society of Chemistry peer review process and has been accepted for publication.

Accepted Manuscripts are published online shortly after acceptance, before technical editing, formatting and proof reading. Using this free service, authors can make their results available to the community, in citable form, before we publish the edited article. We will replace this *Accepted Manuscript* with the edited and formatted *Advance Article* as soon as it is available.

You can find more information about *Accepted Manuscripts* in the Information for Authors.

Please note that technical editing may introduce minor changes to the text and/or graphics, which may alter content. The journal's standard Terms & Conditions and the Ethical guidelines still apply. In no event shall the Royal Society of Chemistry be held responsible for any errors or omissions in this *Accepted Manuscript* or any consequences arising from the use of any information it contains.

ROYAL SOCIETY OF CHEMISTRY

www.rsc.org/njc

Electrosynthesis and electrochemical capacitive behavior of a new nitrogen PEDOT analogue-based polymer electrode

Zilan Feng §, Daize Mo §, Weiqiang Zhou, Qianjie Zhou, Jingkun Xu *, Baoyang Lu *, Shijie Zhen, Zhipeng Wang, Xiumei Ma

School of Pharmacy, Jiangxi Science and Technology Normal University, Nanchang 330013, China

* Corresponding author: Tel: +86-791-88537967; Fax: +86-791-83823320;

Email: xujingkun@tsinghua.org.cn; lby1258@163.com.

§ These authors contributed equally to this work.

In this work, poly(*N*-methyl-3,4-dihydrothieno[3,4-*b*][1,4]oxazine) (PMDTO), a new nitrogen poly(3,4-ethylendioxythiophene) (PEDOT) analogue, was synthesized by electrochemical deposition method and the capacitive properties of PMDTO was investigated and compared with that of PEDOT. The structure and morphology of PMDTO were characterized by Ultraviolet-visible spectroscopy, Fourier transform infrared spectroscopy, scanning electron microscopy, and thermal analysis. The pseudocapacitive properties of as-prepared PMDTO electrodes have been examined by cyclic voltammetry (CV), galvanostatic charge-discharge (GCD) and electrochemical impedance spectroscopy (EIS) in 0.1 mol L^{-1} CH_3CN-Bu_4NBF_4 electrolyte solution. As-prepared PMDTO electrode showed a high specific capacitance of 154.3 F g^{-1} at a discharge current density of 3 A g^{-1} and exhibited

cycling stability with maximal capacitance retention of nearly 71% after 500 cycles at a high current density of 10 A g^{-1}. Additionally, the asymmetrical supercapacitor based on PMDTO electrode and PEDOT electrode exhibited a maximum specific capacitance of 63.5 F g^{-1}, an energy density of 12.7 Wh kg^{-1} at a power density of 0.59 kW kg^{-1}. These results implied that the PMDTO electrode can be used as a potential electrode material for supercapacitors.

1. Introduction

Among conducting polymers (CPs), polythiophenes are among the best investigated and most frequently used conjugated materials. Wide potential applications of CPs have been found in organic electronic devices, such as photonics, nanoarchitectures, chemical and biological sensors, and electrochemical capacitors.[1-3] Among them, poly(3,4-ethylendioxythiophene) (PEDOT), is one of the most extensively researched polymers due to its moderate band gap (1.6 eV), low oxidation potential, high conductivity (easily up to 500 S cm^{-1}), outstanding environmental stability, and compatibility with aqueous electrolytes.[4-6] Especially, its excellent electrochemical behaviors (wide potential range, fast redox transitions and excellent electro-stability), make PEDOT-based materials quite promising in supercapacitors.[7-10]

Supercapacitors (SCs) are emerging as a new class of energy storage devices that exhibiting intermediate properties of high-energy-density batteries, high-power electrolytic capacitors, along with long cycle life, fast charge time, and safe operation mode.[11-12] According to the charge storage mechanism, SCs can be divided into

electrochemical double-layer capacitors (EDLCs) and pseudocapacitors. The mechanism of EDLCs arises from charge accumulation in the electric double layer formed at the electrode/electrolyte interface where the electrode possessing typical carbon materials with large surface area and low matrix resistivity.[11-14] The other, the pseudocapacitors (redox capacitors) do not store charge electrostatically but store charge using fast, reversible, surface or near-surface redox reactions of the electroactive species, typically transition metal oxides or CPs as the electrode materials.[15-17] Among various materials that have been investigated for supercapacitors, CPs are inevitable because of the fast switching between the oxidized and reduced states, high conductivity, environmental friendliness, low cost, and excellent mechanical properties.[18-20]

Although PEDOT was considered as a promising electrode material for supercapacitors, its moderate specific capacitance[21-24] compared with other CPs suggested a need to develop new alternatives. At present, many methods have been developed to improve the capacitive performance of PEDOT, such as constructing composites with nanostructure carbon or metal oxides, microstructure modification, novel dopant schemes, and developing asymmetric devices.[25-29] Nevertheless, in addition to these efforts continuing to advance this field, there is a need to develop new CPs with enhanced faradaic charge storage.

On the other hand, only a finite number of CPs for supercapacitor applications has been investigated so far. Nowadays, many researchers have paid attentions to synthesize new CPs with preferable capacitive performance and higher specific

capacitance values. Recently, Mustafa Güllü and collaborators reported the supercapacitive properties of a series of novel thiophene polymers, which showed a satisfactory supercapacitive performance (poly(5,12-dihydrothieno[3,4:2,3][1,4]dioxocino-[6,7-*b*]quinoxaline (213.7 F g^{-1}), poly(2,3,4*a*,9*a*-tetrahydro[1,4]-dioxino[2,3-*b*]thieno[3,4-*e*][1,4] dioxine) (260 F g^{-1}), *etc.*).[30-32] John R. Reynolds *et al* studied the capacitive behaviors of poly(2,2-dimethyl-3,4-propylene-dioxythipohene) (PProDOTMe$_2$) as polymeric electrodes in Type I electrochemical supercapacitors.[33] This device presented robust capacitive charging/discharging behaviors (85% retained after 32000 cycles) with specific capacitance of 55 F g^{-1}. Poly(3,4-ethylene-dithiothiophene) (PEDTT), the sulfur analogue of PEDOT, with high discharge specific capacity (> 425 mAh g^{-1}, higher than PEDOT (140 mAh g^{-1})), was a promising cathode active material for rechargeable lithium batteries.[34] These investigations indicate that the design and synthesis of the novel thiophene-based conducting polymers or PEDOT analogues and derivatives as alternatives of PEDOT in pseudocapacitor applications are quite feasible.

Poly(*N*-methyl-3,4-dihydrothieno[3,4-*b*][1,4]-oxazine) (PMDTO), a new nitrogen analogue of PEDOT consisting of an electron donating group, dihydro-1,4-oxazine ring similar to dihydro-1,4-dioxine ring of EDOT, was first synthesized by Mustafa Güllu [31] and expected to exhibit electrochemical performance comparable to PEDOT as electrode material in pseudocapacitor applications. As the author stated, PMDTO modified electrodes have more effective electrochemical ability as cathode material

(*n*-dopable electrode) than PEDOT. What amazed us was that the symmetric pseudocapacitor cell based on two PMDTO electrodes showed excellent supercapacitive performance (312.3 F g^{-1}), much better than those results found in the literature up to date for pseudocapacitors constructed with thiophene-based conducting polymers. To the best of our knowledge, it is very difficult for a supercapacitor based on CPs to achieve such high supercapacitive performance. Therefore, the fundamental understanding of the supercapacitive properties of PMDTO is very necessary and significant.

Herein, in this work, we describe the electrochemical polymerization and capacitive properties of PMDTO as polymeric electrodes for supercapacitors. For comparison, the capacitive properties of PEDOT were also investigated under the same conditions. Experiments found that the electrodes based on PMDTO could display higher specific capacitance than PEDOT under the same conditions. Nevertheless, the capacitive properties of PMDTO device are inferior to that of PEDOT device. Furthermore, the structural characterization, morphology and thermal stability of PMDTO films were also minutely investigated.

2. Experimental section

2.1 Chemicals

3,4-Dibromothiophene was purchased from Shanghai Vita Chemical Reagent Co., Ltd. China. 2-(Methylamino)ethanol (Energy Chemical) and *N*,*N*-dimethylethanolamine (DEANOL, Aladdin) were used as received. Acetonitrile

(CH_3CN) were purchased from Beijing Chemical Plant, China and used after reflux distillation. Tetrabutyl-ammonium tetrafloroborate (Bu_4NBF_4) was purchased from Sigma Aldrich and used without further purification. Other reagents were all analytical grade and used directly without further purification unless otherwise noted.

2.2 Monomer synthesis

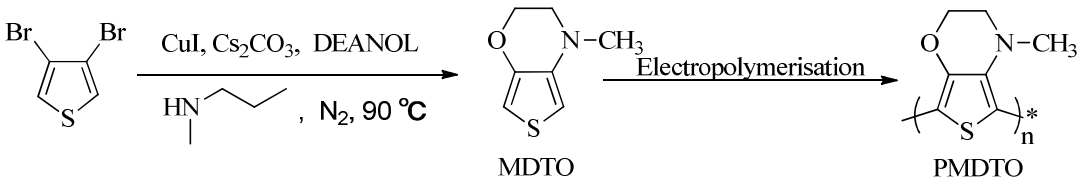

Scheme 1 Strategy for the synthesis of MDTO and the electrosynthesis of PMDTO.

N-methyl-3,4-dihydrothieno[3,4-*b*][1,4]oxazine (MDTO) was synthesized according to previous reported methods.[31] 2-(Methylamino)ethanol (10 mL, excess) was added to a stirred solution in *N*,*N*-dimethylethanolamine (30 mL) containing 3,4-dibromothiophene (1.10 g, 4.55 mmol), copper (I) iodide (0.25 g, 1.31 mmol) and cesium carbonate (4.46 g, 13.7 mmol), and the reaction mixture was allowed to come to 90 ºC. After refluxing for 48 h under nitrogen atmosphere, the reaction mixture was extracted with moderate dichloromethane, washed with brine and combined organic layers, and dried over $MgSO_4$. Purification of the residue was accomplished by chromatography on silica by a silica gel column chromatography using ethylacetate/hexane = 1/20 as an eluent. The product was obtained as light yellow oil that turned brown on exposure to air with time (0.43 g, 60% yield). ^{1}H NMR (400 MHz, $CDCl_3$) δ/ppm: 2.83 (s, 3H), 3.09 (t, J = 4.40 Hz, 2H), 4.28 (t, J = 4.40 Hz, 2H), 5.92 (d, J = 3.20 Hz, 1H), 6.27 (d, J = 3.20 Hz, 1H). ^{13}C NMR (400 MHz, $CDCl_3$)

δ/ppm: 39.64, 48.46, 65.89, 94.94, 98.97, 137.18, 143.53.

2.3 Preparation of PMDTO electrodes

The polymer films were grown potentiostatically on Pt substrates at suitable electrode potential (at + 0.7 V for MDTO, and at +1.4 V for EDOT) in the presence of 0.03 mol L^{-1} monomer in acetonitrile containing 0.1 mol L^{-1} Bu_4NBF_4**.** After electropolymerization, the obtained polymer electrodes were washed repeatedly with monomer free acetonitrile to remove the electrolyte and monomer from electrode surface.

The mass of polymer films (m) was calculated from the total charge passed through the cell during the film growth process, according to *eq.* (1)[35]:

$$m = \frac{(\eta Q_{dep1})M_1}{FZ_1} \qquad (1)$$

Here, m is calculated by using the charge (Q_{dep1}), assuming a 100% current efficiency (η) (the total charge passed through the cell during the polymer film growth process). M_1 is the molecular weight of MDTO or EDOT, F is the Faraday constant (96,485 C/mol). Z_1 is the number of electrons transferred per monomer attached to the polymer, in which $Z_1 = 2 + f$ [36]. The partial charge f is called the doping level, the calculated f was about 0.22 for PMDTO and 0.33 for PEDOT in the experiments, assuming a 100% current efficiency (η), according to *eq.* (2) [37]:

$$f = \frac{2Q_0}{Q_d - Q_0} \qquad (2)$$

Where Q_d is the total charge used for polymer deposition, and Q_o is the total charge of oxidized species in the polymer films.

We have validated the reproducibility of mass through calculation of *eq.* (1) through five parallel experiments. To obtain a sufficient amount of polymer for weighing, we used Pt sheet with a surface area of 5 cm^2 as working electrode. Namely, after deposition of polymers, the polymers were washed repeatedly with anhydrous CH_3CN to remove the supporting electrolyte and un-reacted monomer. Then, the Pt sheet coated polymer films were dried under vacuum at 60 °C for 24 h to remove the solvent. The mass of PMDTO and PEDOT deposited on Pt sheet was weighed out using a micro-analytical balance. The calculated standard deviation is about 3.3% through five parallel experiments. The mass calculated through *eq.* (1) is about 10% higher than that obtained by weighing method. In this paper, the mass calculated through *eq.* (1) was used to obtain the specific capacitance. The amount of PEDOT and PMDTO was similar, was 10.11 μg and 10.27 μg, respectively.

To obtain a sufficient amount of the polymer films for characterization, ITO-coated glasses were employed as the working electrode and another Pt sheet was used as the counter electrode. They were placed 5 mm apart during the examinations. Prior to each experiment, the ITO electrodes were immersed in ethanol for 6 h and ultrasonically cleaned for 15 min, then cleaned successively with water and acetone, and then dried in air. An Ag/AgCl electrode directly immersed in the solution served as the reference electrode, and it revealed sufficient stability during the experiments. The polymer was deposited on ITO electrodes by potential method at suitable electrode potential (at + 0.7 V for MDTO, and at +1.4 V for EDOT) in the presence of 0.03 mol L^{-1} monomer in acetonitrile containing 0.1 mol L^{-1} Bu_4NBF_4.

2.4 Fabrication of the pseudocapacitor cells

Asymmetric supercapacitor cell was assembled by using PMDTO modified Pt electrode as anode and PEDOT modified Pt electrode as cathode. Symmetric supercapacitor cells were assembled by using two PEDOT modified Pt electrodes as both the anode and cathode active materials. A two electrode configuration was set up in both the symmetric and asymmetric type pseudocapacitor cells (The distance of two electrodes is fixed at about 5 mm). The polymer coated Pt electrodes were placed in cylindrical glass cell (30 mm ×60 mm) filled with 0.1 mol L^{-1} acetonitrile-tetrabutylammonium tetrafloroborate (CH_3CN-Bu_4NBF_4) supporting electrolyte system and sealed with a plastic stopper. All symmetric pseudocapacitor cells (Cell 1 and Cell 2) were constructed by using this procedure.

Configuration of pseudocapacitor cells:

Cell 1: PMDTO modified Pt/0.1 mol L^{-1} CH_3CN-Bu_4NBF_4/PEDOT modified Pt

Cell 2: PEDOT modified Pt/0.1 mol L^{-1} CH_3CN-Bu_4NBF_4/PEDOT modified Pt

2.5 Characterization

The surface morphologies of PMDTO electrode materials were characterized by field-emission SEM (FE-SEM, JSM-6330F). Infrared spectra were determined with a Bruker Vertex 70 Fourier-transform infrared (FT-IR) spectrometer with samples in KBr pellets. Ultraviolet–visible spectroscopy (UV-vis) was measured on a UV–vis spectrophotometer (SPECORD 200). The thermogravimetric analysis (TGA) was performed with a thermal analyzer of NETZSCH TG209 under a nitrogen stream in the temperature range of 295-1173 K with a heating rate of 10 K/min. Cyclic

voltammetry (CV), galvanostatic charge–discharge, and electrochemical impedance spectroscopy (EIS) measurements were conducted using an electrochemical workstation (CHI 660B). The electrochemical studies of the individual electrode were performed in a three-electrode cell, with a Pt counter electrode and an Ag/AgCl reference electrode. All the electrochemical measurements for electrodes were performed in 0.1 mol L^{-1} CH_3CN-Bu_4NBF_4 supporting electrolyte system at room temperature. All the measurements were measured using a CHI 660B electrochemical workstation. The EIS measurements were recorded under AC voltage amplitude of 5 mV, a frequency range of 10^5 to 0.01 Hz, and an open circuit potential of 0.7 V (*vs* Ag/AgCl).

2.6 Details of computations

All calculations were carried out using the Gaussian 03 program.[38] The structure of the trimmers were optimized without symmetry constraints using a hybrid density functional[39,40] and Becke's three-parameter exchange functional combined with the LYP correlation functional (B3LYP)[41,42] using the 6-31G(d,p) basis set (B3LYP/6-31G(d,p)). Vibrational frequencies were evaluated at the same level to identify the real minimum energy structures.

3. Results

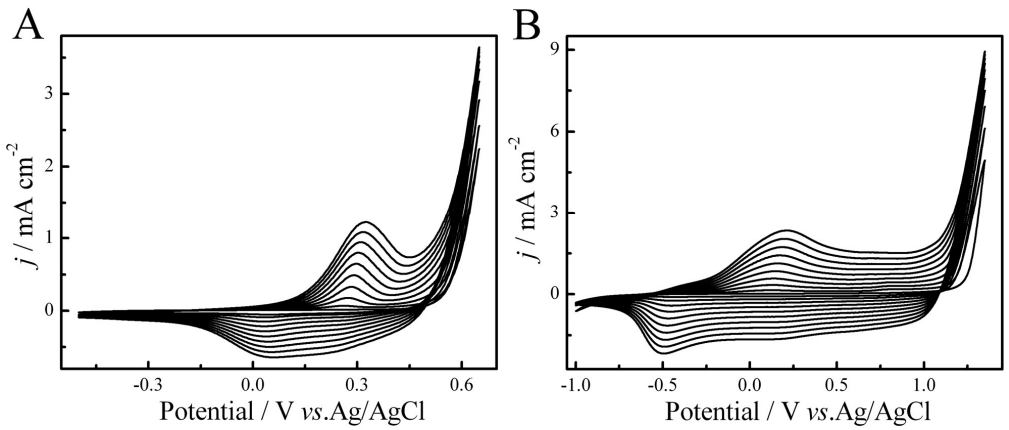

Fig. 1 Cyclic voltammograms of 0.03 mol L^{-1} MDTO (A) and EDOT (B) in 0.1 mol L^{-1} CH_3CN-Bu_4NBF_4 at the scan rate of 100 mV s^{-1} (j = current density).

Fig.1 shows the successive CV curves of 0.03 mol L^{-1} MDTO in CH_3CN-Bu_4NBF_4 between -0.5 and 0.65 V at a potential scan rate of 100 mV s^{-1}. As shown in Fig. 1A, the onset oxidation potential ($E_{pa,\ onset}$) of MDTO in the solution is +0.57 V *vs* Ag/AgCl, which is lower than that of EDOT (+1.24 V *vs* Ag/AgCl) (Fig. 1B), thieno[3,4-b]-1,4-oxathiane (EOTT) in CH_3CN-Bu_4NPF_6 (0.1 M) (nearly +1.2 V *vs* Ag/AgCl), [43] 3,4-ethylenedithiothiophene (EDTT) in $BmimPF_6$ (+0.93 V *vs* Ag/AgCl).[44]

This is a surprising phenomenon for that the insertion of nitrogen that is less electronegative than oxygen but lowers the oxidation potential so much. Combined with the experimental results and previous reported results, we made the following assumptions: the cooperation of the strong electron-donating properties of the nitrogen atom and the methyl groups, [45] the conjugation of the p-π* and π-π* transitions and the more facilely formation of ammonium cationic radicals. As is known, the heteroatom proved to play an important role in tuning the properties of the

resulting conjugated polymers. It is also reported that the onset electrochemical oxidation potentials of 3,4-methylenedithiopyrrole, [46] 3,4-ethylenedioxypyrrole (EDOP), [47] 3,4-ethylenedithio-pyrrole, [48] and 3,4-alkylenedioxypyrroles (XDOPs) [49] were lower than those corresponding EDOT variants. From another point of view, the low potential would provide considerably milder polymerization conditions and would be in favor of yielding a high quality polymer. [50] Hence, the replacement of oxygen atom by nitrogen atom would have a positive effect on the final PMDTO films.

The polymerization of MDTO presents an oxidation peak at +0.32 V and a board reduction peak at +0.15 V. As the CV scan continues, PMDTO polymers were formed on the working electrode surface. In the cathodic scan process, the shift of peak potentials implied the increase of electrical resistance in the polymer film and the overpotential required to overcome this resistance. The apparent reduction peaks may be assigned to the transformation from the quinoid structure to the aromatic state. [51] The increase in the oxidation/reduction wave current densities indicated that increasing amount of conducting polymers was deposited on the electrode. A similar phenomenon was also observed during the electro-polymerization of EDOT in CH_3CN-Bu_4NBF_4 (Fig. 1B).

In this work, the PEDOT and PMDTO films were all prepared by the potentiostatic method at certain potential (EDOT: +1.4 V *vs* Ag/AgCl, MDTO: +0.7 V *vs* Ag/AgCl). For SEM, UV-vis, FT-IR, and thermal characterizations, polymer films were deposited on ITO-coated glass for a certain time. Before electrochemical test, the

resulting PEDOT and PMDTO films were rinsed with monomer-free CH_3CN solution repeatedly, and then transfered to another cell for the test.

The scan electron microscope (SEM) (Fig.S1) of PMDTO showed very sponge-like structure morphology, which was different from the heterogeneous and porous morphology of PEDOT. [7] This morphology might facilitate the movement of doping anions into and out of the polymer film during the doping and de-doping process, [31] which is an ideal surface morphology for pseudocapacitor applications. The film thickness (Fig.S2) showed that the film thickness of PMDOT and PEDOT were about 0.8 μm and 1.0 μm, respectively.

The UV-vis absorption spectra of MDTO monomer in CH_3CN solution and the corresponding polymer films deposited on ITO electrode are shown in Fig.2. The absorption maxima for MDTO monomer (a) is 278 nm, lying between EDOT (258 nm), 3,4-ethylenediselenathiophene (EDST) (282 nm) and 3,4-ethylenedithiathiophene (EDTT) (289 nm), [52] representing the substituent effect of different heteroatoms and substituents toward the π-π* transition. Meanwhile, the λ_{max} of PMDTO (b) was observed at about 465 nm, with a blue shift of about 111 nm to PEDOT (576 nm). This is possibly attributed to the increasing planarity of the polymer chains (PEDOT > PMDTO, spectra obtained from thin films). In addition, the bathochromic shift (307 nm) of PMDTO when compared with the monomer indicates the occurrence of electrochemical polymerization among the monomers and the formation of a conjugated polymer with longer effective conjugation length.

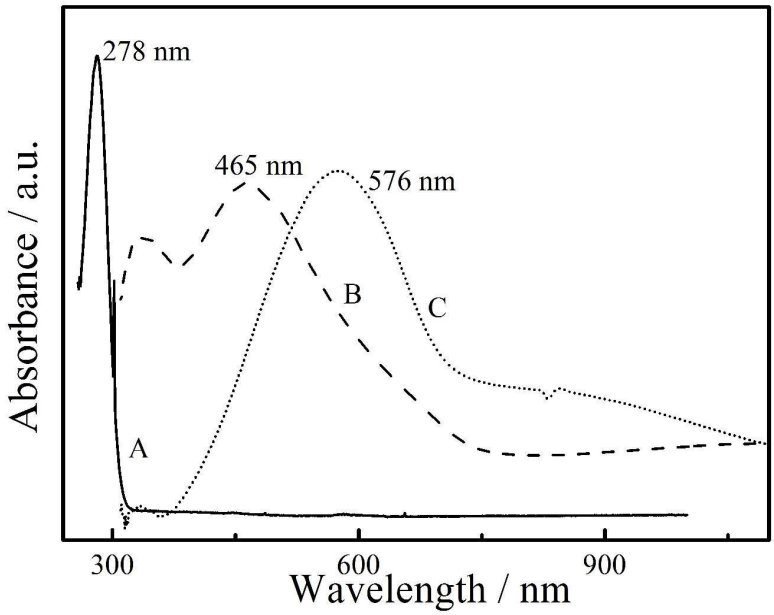

Fig. 2 UV-vis spectra of MDTO monomer (A) and the de-doped PMDTO (B) and PEDOT (C) film on ITO electrode at -1.0 V *vs* Ag/AgCl.

To obtain a further interpretation of polymers, including planar structure, HOMO-LUMO levels, and band gap, density functional theory calculations have been performed. Quantum chemical calculations were performed on the trimers: (EDOT)3, 3,4-dihydro-2H-thieno[3,4-b][1,4]oxazine (D[2H]TO)3, and (MDTO)3 using the Gaussian 03 suite of programs (Fig.3). Geometry optimization at the B3LYP/6-31G(d) level predicts a highly planar structure for (EDOT)3, the optimized dihedral angles between the planes of the thiophene units was 178° (close to 180°). This indicates the highest possible π-electron coupling, which lowers the HOMO-LUMO gap of the corresponding polymers, allowing the preparation of conjugated polymers with enhanced main chain planarity and higher electrical conductivity. When one oxygen atom was replaced by nitrogen atom [(D[2H]TO)3], these angles are 160°, the structure is less planar. In (MDTO)3, the dihedral angle opens to 108°, giving a highly

nonplanar structure. All these results indicated that the difference in the ethylene bridge would decrease planarity of the corresponding polymers. We repeated the geometry optimizations starting from planar structures, but in all cases, the same structures were obtained.

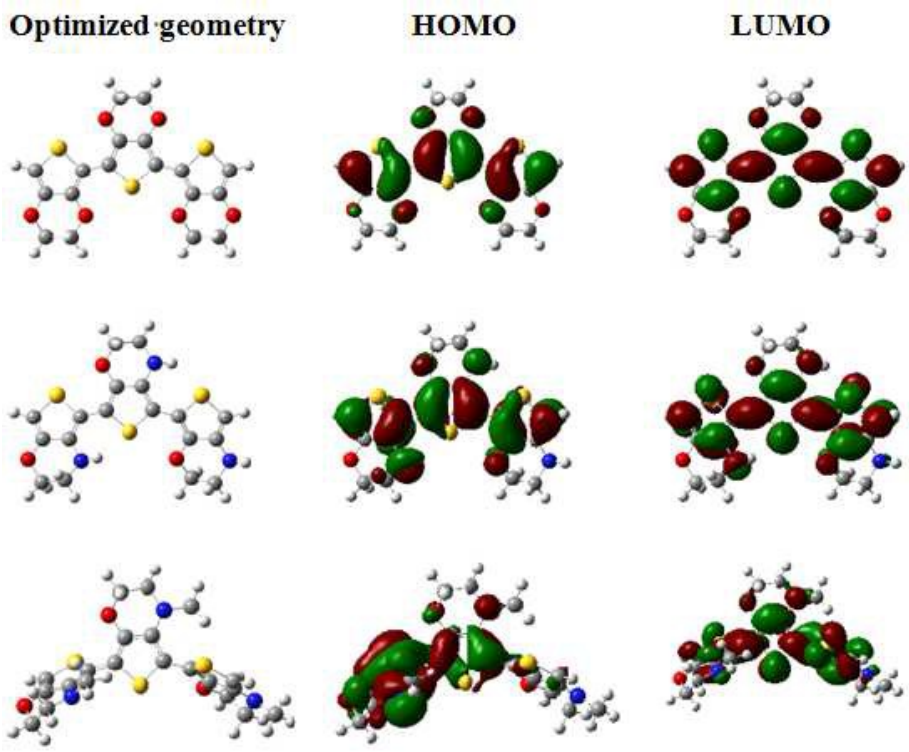

Fig. 3 Optimized structures and HOMO-LUMO levels of (EDOT)3, 3,4-dihydro-2H-thieno[3,4-b][1,4]oxazine (D[2H]TO)3, and (MDTO)3.

FT-IR spectroscopy is carried out over a range of 400-4000cm^{-1} to further interpret the polymerization mechanism and the chemical structure of PMDTO, FT-IR spectra of MDTO and PMDTO were recorded, as shown in Fig. S2. FT-IR spectrum of PMDTO shows the following absorption peaks: 2962-2875 cm^{-1} (aliphatic C-H stretching), 1524, 1488 cm^{-1} (aromatic C=C stretching), 1327 cm^{-1} (C–C stretching), 1276, 1162, 1130 cm^{-1} (C-O-C stretching), 677 cm^{-1} (C-S stretching). It is clear that

the strong bands ascribed to the =C-H stretching vibration at 3109 cm^{-1} and the absorption band at 774 cm^{-1} arising from C-H_α stretching of the thiophene moiety of MDTO monomer (a) disappeared completely. This is an evidence of the polymerization from 2, 5 positions of the thiophene moiety of the monomer. The broad band observed at around 1639 cm^{-1} was due to polyconjugation.[53] The strong absorption peak at 1087 cm^{-1} was attributed to the incorporation BF_4^{-1} into the polymer films during the doping process.[54] The FT-IR results of PMDTO clearly indicated the successful electropolymerization of the monomers.

Thermal properties of PMDTO were determined by thermogravimetric analysis (TGA) under nitrogen atmosphere at a heating rate of 10 K min^{-1}. An initial weight loss of about 5% was closely related to evaporation of bound water present in the polymer matrix. As shown in Fig. S3, as-prepared PMDTO polymer has good thermal stability with onset decomposition temperature at 511 K, and a maximal decomposition temperature appeared at 600 K. There was a three-step loss of weight. The first one is slight from 300 to 511 K (about 5%), resulting from evaporation of water or other moisture trapped in PMDTO. [1] The second one occurred from 511 to 677 K, up to 27.28%, which may be due to the degradation of the skeletal backbone chain structure. The last one was about 17.14% from 677 to 1081 K, probably owing to the overflow of some oligomers decomposing from PMDTO with the increase of the temperature.

No well-defined plateau even under high temperature is a common phenomenon for conducting polymers, such as poly(1,2-methylenedioxybenzene) (PMDOB), [55]

poly(indole-5-carboxylic acid) (PICA), [56] polyselenophene,[57] and poly(9,10-dihydrophenanthrene) (PDHP), [58] etc. Such phenomena indicated that the polymers could be further decomposed to some extent under higher temperature. Obviously, the thermal stability of PMDTO is adequate for its applications in supercapacitors and other optoelectronic devices such as electrochromic device.

To explore the performance PMDTO in supercapacitors, cyclic voltammetry measurements were performed in a three-electrode configuration with a Pt wire as counter electrode and an Ag/AgCl electrode as reference electrode in CH_3CN solution containing 0.1 mol L^{-1} Bu_4NBF_4. The cyclic voltammograms (CVs) of PMDTO among -0.3-1.0 V *vs* Ag/AgCl (PEDOT: -0.9-1.2 V *vs* Ag/AgCl) at sweep rates of 25-200 mV s^{-1} are shown in Fig.4. The CVs of PMDTO (Fig. 4B) show two pairs of redox peaks, indicating that the capacitance of PMDTO mainly results from pseudocapacitance mechanism rather than that of double-layer capacitance (also for PEDOT). PMDTO polymer exhibits a considerably higher oxidation potential (0.7 V higher than PEDOT, Fig. 4B) when compared with PEDOT, possibly attributed to a large torsion angle between the repeated units in the electroneutral polymer chain and considerably weaker chain ordering through sulphur-nitrogen interactions in contrast to sulphur-oxygen ones in PEDOT. [59] It can be seen that the current intensity of both PMDTO and PEDOT increases as the scan rate increases, and the potentials of the oxidation and reduction peaks shift to more positive and negative directions. These are attributed to an increase in the charge diffusion polarization within the pseudoactive material when the scan rate increases. The peak currents are plotted as a

function of sweep rate (υ) and $\upsilon^{1/2}$, respectively (Fig. 4C and Fig. 4D). As can be seen that the peak currents versus υ plots exhibit a linear relationship, which indicated that the electrochemical behavior of PMDTO electrode was an adsorption controlled process rather than diffusion controlled. [60]

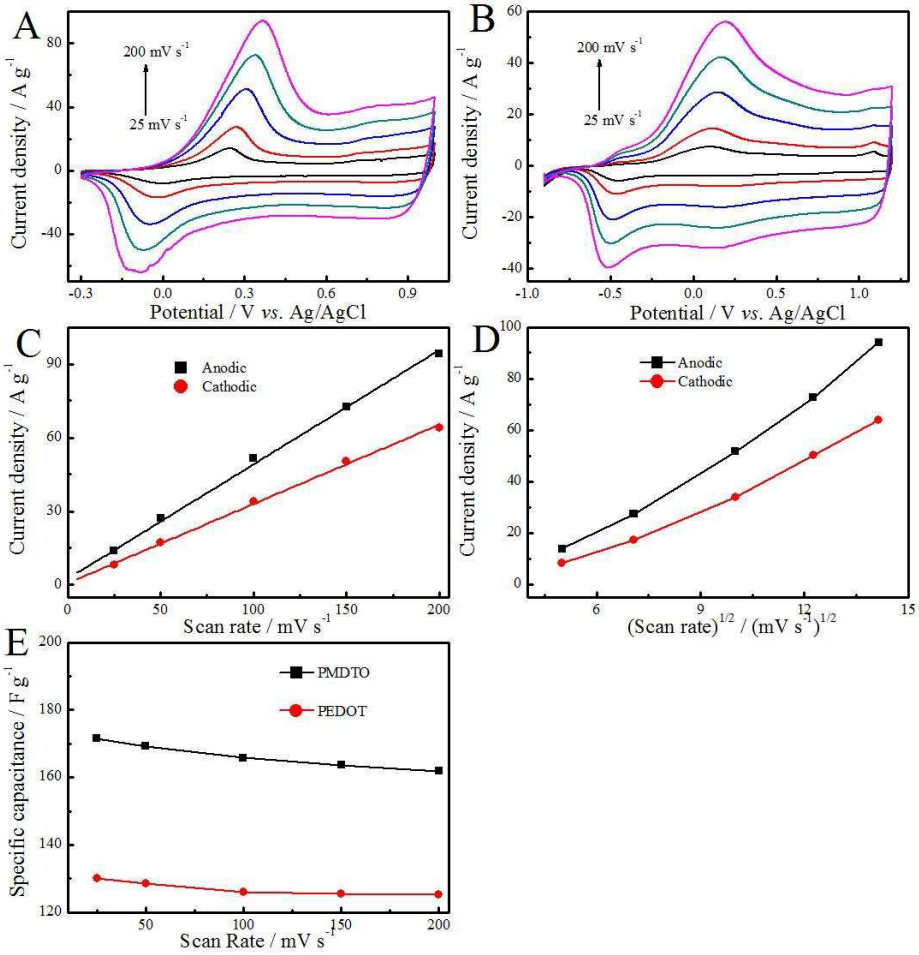

Fig. 4 Cyclic voltammograms of PMDTO (A) and PEDOT (B) modified electrodes in 0.1 mol L^{-1} monomer-free CH_3CN-Bu_4NBF_4 at potential scan rates of 200, 150, 100, 50, and 25 mV s^{-1}; (C) redox peak current of PMDTO electrode as a function of scan rate; (D) redox peak current of PMDTO electrode as a function of $(\text{scan rate})^{1/2}$; (E) specific capacitance of PMDTO and PEDOT as a function of scan rate

The specific capacitance was calculated from CV curves according to the following equation[61]:

$$C_s = \frac{q_a + q_c}{2mv\Delta V} \quad (1)$$

Where C (F g^{-1}), q_a, q_c, v (V s^{-1}), m (g), and ΔV (V) are the specific capacitance, the sums of anodic and cathodic voltammetric charges on the anodic and cathodic scans, the scan rate, the mass of the active material, and the potential range of CV, respectively. On the basis of the equation, the specific capacitance of PMDTO and PEDOT at the scan rates of 25, 50, 100, 150, and 200 mV s^{-1} were calculated. It can be observed that the specific capacitance of PMDTO electrode is 171.5 F g^{-1} at the scan rate of 25 mV s^{-1}, which is higher than 130.2 F g^{-1} of PEDOT electrode at the same scan rate. Fig. 3E shows the dependences of specific capacitance of PMDTO and PEDOT on their scan rates. The PMDTO electrode shows about 13.7% decay (20.6% for PEDOT) as the scan rate increases from 25 mV s^{-1} to 200 mV s^{-1}. And the specific capacitance of PMDTO can still retain 161.9 F g^{-1} at the scan rate of 200 mV s^{-1}, also higher than PEDOT (125.2 F g^{-1}). Therefore, the above results indicate that PMDTO electrodes have a higher specific capacitance than PEDOT at various scan rates, and could be considered to be promising electrode materials for supercapacitors. From these results, we can also conclude that the specific capacitance of the PMDTO electrode is competitive when compared with many other traditional conducting polymers, such as such as polythiophene (PTh) (117 F g^{-1}), [62] polypyrrole (PPy) (186 F g^{-1}), [63] polyaniline (PANI) (216 F g^{-1}), [64] and polyselenophene (PSe) (72.2 F g^{-1}). [65]

To learn more about the charge storage capacity of the electrodes, galvanostatic

charge-discharge (GCD) measurements was carried out as shown in Fig. S5. The specific capacitance of PMDTO electrode was performed using a potential window of -0.3-1.0 V and compared with PEDOT electrode (Fig. S5A). A non-linear variation of potential versus time (Fig.S5A) illustrates a typical pseudocapacitance performance resulting from the electrochemical redox reaction occurred at the PMDTO electrode/electrolyte interface, which is well in agreement with the analysis about the CV curves. In addition, galvanostatic charge-discharge curves of PMDTO exhibits a pair of voltage plateaus at around 0.03 and -0.12 V, which is consistent with the above CV analysis. The charge plateau region and discharge plateau region of PMDTO is owing to the oxidation reactions (doping) and reduction reactions (de-doping) of PMDTO. [66]

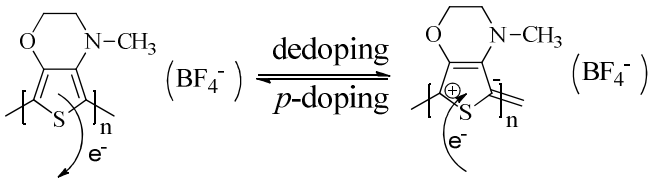

Scheme 2 The doping and de-doping process of PMDTO.

Rate capability is one of the important factors for evaluating the power applications of supercapacitors. The specific capacitance obtained from galvanostatic charge/discharge method was calculated according to the following equation: [67]

$$C = \frac{I\Delta t}{m\Delta V} \qquad (2)$$

Where ΔV (V) represents the discharge potential range, I (A) is the constant charge or discharge current density, m (g) is the mass of the active material, and Δt (s) is the corresponding discharge time. Based on the above formula, the specific capacitance of

PMDTO is 154.3 F g^{-1} at a current density of 3 A g^{-1}, which is higher than the value of 134.6 F g^{-1} for PEDOT investigated under the same conditions. The higher capacitance of PMDTO was mainly attributed to the decrease of oxidation onset potential of MDTO (the low potential would provide considerably milder polymerization condition and be in favor of yielding a high quality polymer) and sponge-like structure morphology (an ideal surface morphology for pseudocapacitor applications), which was different from the compact and smooth surface morphology of PEDOT [68]. According to the charge-discharge curves at various current densities, the specific capacitance is calculated and plotted in Fig.S5C, and the reduction of specific capacitance at large current density can be obviously observed. Even so, when the current density increases to 35 A g^{-1}, the specific capacitance of PMDTO remains to be 124.4 F g^{-1} (about 19.5% decrease from that at 3 A g^{-1}), further confirming its good rate capability. However, as expected, the rates capability of PEDOT is better than PMDTO (about 8.0% decreases from 3 A g^{-1} to 35 A g^{-1}).

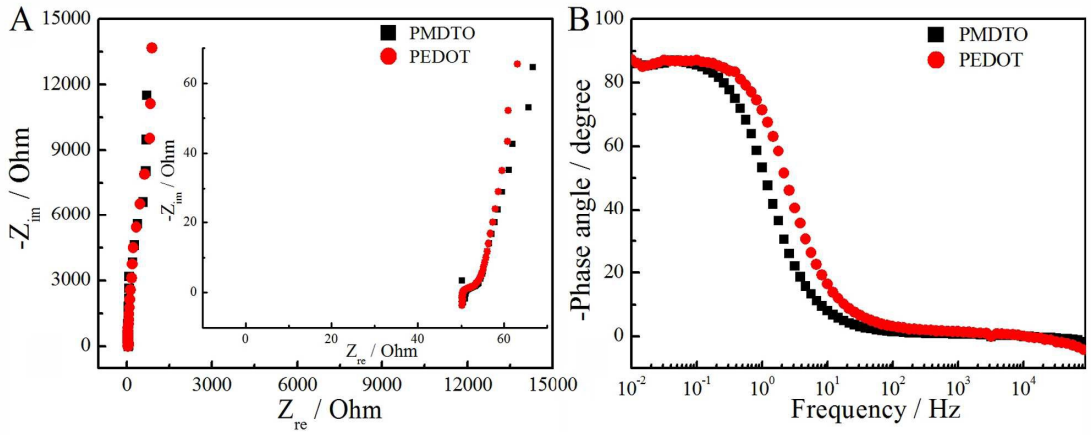

Fig. 5 Impedance spectra of PMDTO and PEDOT modified electrodes in CH_3CN-Bu_4NBF_4: (A) Nyquist plots; (B) Bode-phase angle plots. Electrode potential:

1.0 V.

Electrochemical impedance spectroscopy (EIS) was also conducted to investigate the electrochemical property of the PMDTO and PEDOT electrodes. EIS is a powerful tool for mechanistic analysis of an interfacial process and the evaluation of rate constant, ionic and electronic conductivity, and double-layer capacitance, *etc*. All the plots display a semicircle in the high frequency region and a straight line in the low-frequency region (Fig.5A). The intercept at the real axis of the plot corresponds to the solution resistance (R_s), and their values are very similar (52.52 Ω for PMDTO, 52.43 Ω for PEDOT). The slope of a straight line in the low frequency region reflects the diffusive resistance resulting from the diffusion of active species in the electrolyte. As shown in Fig.5A, the PMDTO electrode shows almost a vertical line in the low frequency region, indicating small diffusive resistance of the electroactive species in the electrolyte. The size of the semicircle was determined by the charge transfer resistance (R_{ct}) at the interface between the electrode material and the electrolyte. Here, the value of R_{ct} for PMDTO is 4.93 Ω, close to that of PEDOT (4.8 Ω), indicating that the conductivity of PMDTO is competitive to PEDOT. In the phase angle plot (Fig. 5B), the approaching to pure capacitive behavior at low frequency is usually identified with phase angle approaching to -90º. The phase angle of PMDTO electrode reached -86.2º at 0.01 Hz, very close to that of PEDOT electrode (-87.3º). All these results show the good electrochemical capacitive properties of the PMDTO electrode and its potential applications in supercapacitors.

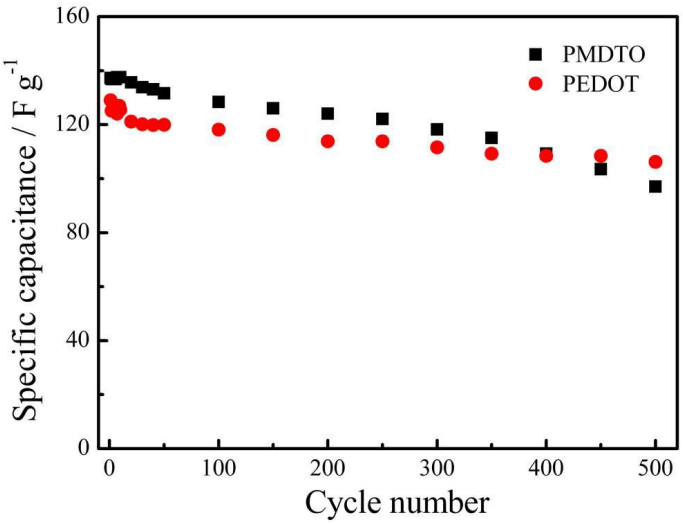

Fig. 6 Galvanostatic charge-discharge life of the electrodes in CH_3CN-Bu_4NBF_4 at the constant current density of 10 A g^{-1}.

A long cycle-life is an important factor for practical supercapacitor applications. However, one significant drawback of organic electrode materials is their insufficient electrochemical stability. Here, the cycling performance of PMDTO and PEDOT electrodes were evaluated by 500 charge-discharge cycles between -0.3 and 1.0 V at the current density of 10 A g^{-1}. Fig.6 depicts the specific capacitance of PMDTO and PEDOT electrodes against cycle number. The value of capacitance dropped ~29% from 137.3 to 97.0 F g^{-1} after 500 cycles, worse than the cycling stability of PEDOT electrode (82.2% retention after 500 cycles). After 1000 cycles, the retention of PMDTO was only 12.3%. The fast decrease in the specific capacitance of PEDOT electrode possibly results from the broad working potential window of the electrode (The electrochemical activity of each ECP is strictly determined by its working potential range limited by an isolating state and/or polymer degradation caused by overoxidation) [69]. The working potential range of PMDTO is also limited, when the

potential was over 1.2 V, the electrochemical activity of PMDTO was lost quickly). In general, the stability of conducting polymers could be a serious problem because of typical shrinkage, breaking, cracks, and overoxidation appearing in subsequent cycles, that is connected with volumetric changes of the polymer during intercalation of counter ions. [21]

To verify the feasibility of as-prepared electrodes for supercapacitors, the asymmetric PMDTO/PEDOT device (the measurements of symmetrical PMDTO device could not be completed (Fig.S7)) and symmetrical PEDOT device were presented in Fig. 7. The symmetrical device based on PMDTO is unsuccessful is possibly that the p-doped PMDTO is only suitable as positive materials for supercapacitors. For the symmetrical capacitor based on PMDTO, when it is charged, the positive material PMDTO is partial doped due to the negative material PMDTO simultaneously becomes partial even fully dedoped, which results in the poor performance of the device. So when the voltage is controlled between 0 V and 1.0 V, the poor performance of the device is more serious. However, PEDOT is a good p/n-doped conducting polymer, which is suitable as positive and negative materials for supercapacitors. Fig.7A shows the CVs of the asymmetric PMDTO/PEDOT device at various scan rates. The oxidation peaks and reduction peaks on the CVs can be observed and the peak current becomes larger with the scan rate increasing from 25 to 200 mV s^{-1}. On the contrary, the CVs of PEDOT device has a nearly rectangular shape over the potential window and without obvious anode and cathode peaks (Fig.7B). For both the supercapacitors, there is no obvious distortion even at a high

scan rate of 200 mV s^{-1}, indicating the good fast charge-discharge properties of the devices. [70] In order to further evaluate the performance of the device, we also performed the galvanostatic charge-discharge test at various current densities. Fig.7C and Fig.7D shows the galvanostatic charge-discharge curves of the PMDTO/PEDOT device and PEDOT device at different current densities, respectively. Both their discharge curves tend towards triangular-shaped shapes, and are nearly symmetric with the corresponding charge counterparts, suggesting good electrochemical reversibility. [71] The discharge curve of PMDTO/PEDOT device is substantially prolonged over PEDOT device, suggesting the better capacitive behavior of PMDTO/PEDOT device. Fig.7E displays the specific capacitance at different current densities calculated from discharge curves according to equation (2). Here, the specific capacitance is calculated using the total mass of active materials on both two electrodes. Similar to the results in the three-electrode test, the PMDTO/PEDOT device (63.5 F g^{-1} at 1 A g^{-1}) exhibits significantly enhanced supercapacitive performance comparing with that of PEDOT device (45.1 F g^{-1} at 1 A g^{-1}). The specific capacitance decreases as the current increases, for the same reason as the electro-performance in the three-electrode system. This is due to the fact that high current makes more active material insufficient in the redox reaction as the scan rate increases.[72]These values are lower than those reported for chemically modified graphene supercapacitors (~99 F g^{-1}) [73] and those supercapacitors fabricated by nanocomposites of PEDOT and inorganic materials (e.g., MoO_3, carbon nanotubes, MnO_2, and $NiFe_2O_4$), whose specific capacitance ranged from 198 to 375 F g^{-1}. [74-77]

For practical application of the supercapacitors, power density (*P*) and energy density (*E*) are the most important parameters to evaluate their electrochemical performance. The *P* and *E* of the supercapacitor device were evaluated by the galvanostatic charge/discharge curves and plotted on the Ragone diagram, as shown in Fig. 6F. The values were calculated by the following relationship (3) & (4):

$$E = \frac{1}{2} C(\Delta V)^2 \qquad (3)$$

$$P = \frac{\mathrm{E}}{\Delta \mathrm{t}} \qquad (4)$$

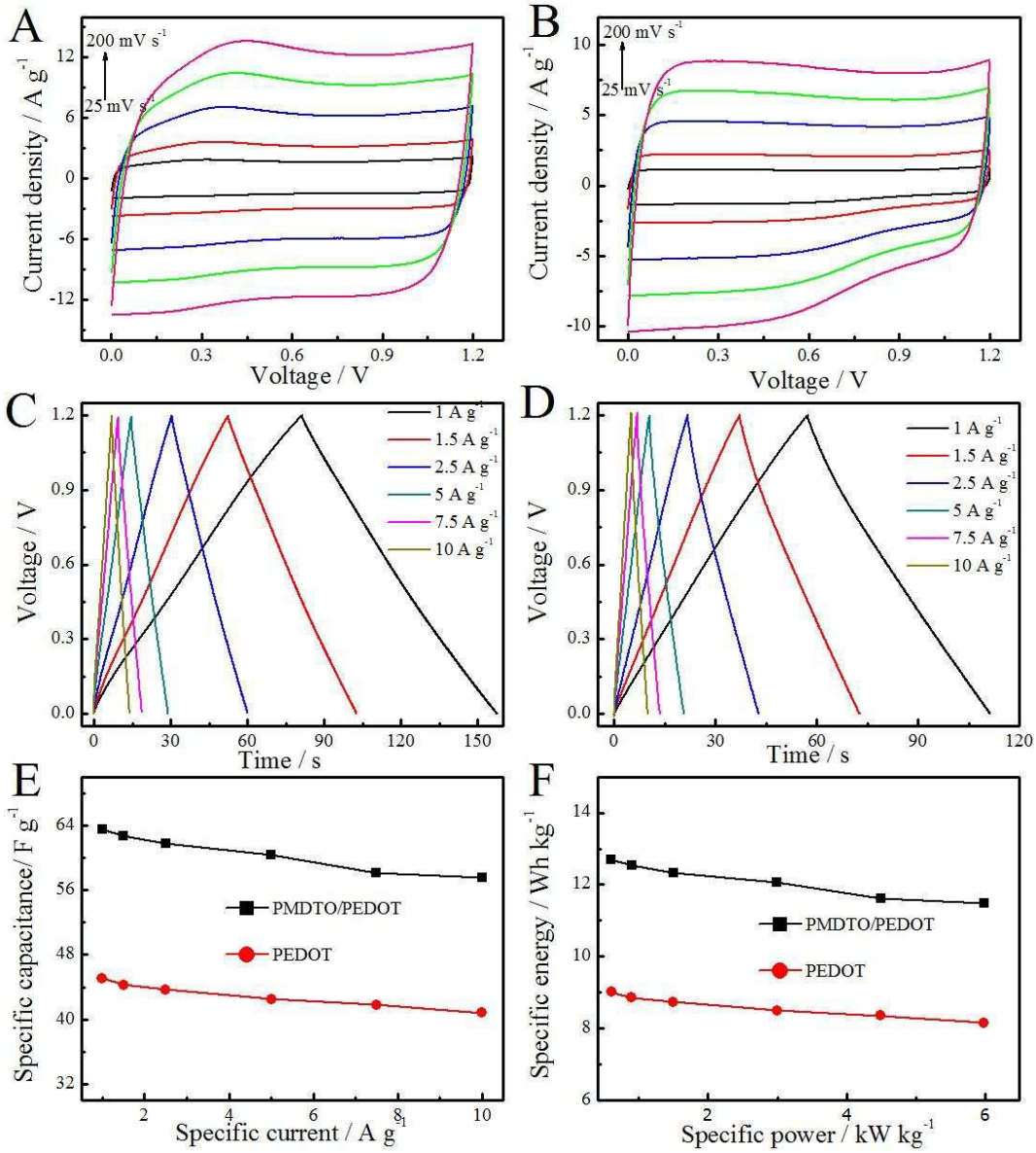

Fig.7 Cyclic voltammograms of a asymmetric supercapacitor based on one PMDTO electrode and one PEDOT electrode (PMDTO/PEDOT) (A) and a symmetric supercapacitor based on two PEDOT electrodes (B); Galvanostatic charge/discharge curves of PMDTO/PEDOT device (C) and PEDOT device (D); (E) specific capacitance calculated from discharge curves of the supercapacitor device; (F) ragone plots of the supercapacitor device.

Where C is the specific capacitance of the electrode, ΔV is the potential window (V), E is the specific energy (Wh kg^{-1}), P is the specific power (kW kg^{-1}), and Δt is the discharge time (s). As anticipated, the specific energy decreases, while the specific power increases as the current increased from 1 to 10 A g^{-1}. As the GV charge/discharge current increases from 1 to 10 A g^{-1}, the specific energy of the PMDTO/PEDOT asymmetric device decreases from 12.7 to 11.5 Wh kg^{-1}, while the specific power increases from 0.59 to 5.99 kW kg^{-1}. For comparison, PEDOT device has smaller specific energy (from 9.0 to 8.1 Wh kg^{-1}) with corresponding specific power from 0.59 to 5.99 kW kg^{-1}. From these results, we can know that the PMDTO/PEDOT asymmetric device and PEDOT symmetrical device is superior to that of many commercial supercapacitors (typically 5-10 Wh kg^{-1}).[79]

4. Discussion

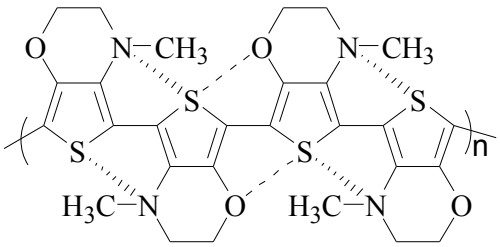

Scheme 3. Diagrammatic representation of S-N and S-O Intramolecular Interactions in PMDTO Backbone

Overall, a new nitrogen analog EDOT-MDTO possesses a more atom-economically synthesis route by one-step procedure than other analogues that require two or more than two procedures, such as EDOT, EDTT, and EOTT, *etc*. The $E_{pa,\ onset}$ of MDTO is +0.57 V *vs* Ag/AgCl, which is lower than that of its analogues. The cooperation of the strong electron-donating properties of the nitrogen atom and the methyl groups, the conjugation of the p-π* and π-π* transitions, or the more facilely formation of ammonium cationic radicals might provide explanation for the very low oxidation potential of MDTO.

The surface morphology of PMDTO films (sponge-like structure morphology) was very different from the morphology of PEDOT. The UV-vis results show that PMDTO has hypsochromic shift (maximum absorption) in the de-doped state than PEDOT. The reasons accounting for this phenomenon are as follows: S···N steric repulsion among adjacent MDTO monomer units leads to the distortion of the π-conjugated backbone, and this disparity is owed more to the conformation of the polymers than the inductive and resonance effects of the chalcogen substituent. This results in the shortening of the effective conjugation length and probably poor solid state ordering.[80] The expected S···N interactions in segments of all-anti conformers are shown in Scheme 3. To sum up, the partial replacement of oxygen by nitrogen atom results in a hypsochromic shift λ_{max} arising from the decreased rigidity of the conjugated structure compared to PEDOT.

We have carefully studied the capacitance performance of PMDTO and PEDOT by means of CV, GCD, and EIS techniques under ambient conditions. PMDTO has shown a higher oxidation potential (0.7 V higher than PEDOT), probably owing to the insertion of nitrogen atoms in the PMDTO chain, which greatly affects the inter-ring conjugation. In addition, the stronger electron-withdrawing effect from the oxygen atoms in PEDOT will promote to decrease the reduction potential. As a supercapacitor electrode, the specific capacitance of PMDTO electrode is higher than PEDOT electrode at various scan rate and specific current. However, PMDTO electrode shows a much smaller potential window and poorer stability compared with that of PEDOT electrode. As the energy density is proportional to the specific capacitance and the square of the operating voltage range, although the specific capacitance of PMDTO is superior to that of PEDOT, PMDTO is not competitive in comparison with PEDOT, combined with its poor stability. And the advantages of PEDOT were further confirmed by the electrochemical results of the symmetrical supercapacitor devices. The tests of PMDTO symmetrical device in the voltage of 0-1.0 V could not be completed, but the CVs of PEDOT symmetrical device is normal during the experiments. In order to overcome the obstacle, we constructed asymmetric PMDTO/PEDOT device, which shown satisfying capacitance performances.

Above all, we can concluded that as a new analogue of PEDOT, PMDTO has some advantages for supercapacitor, such as low oxidation potential of the monomer and relatively higher specific capacitance values, but it also suffered from the problems of decreased rigidity, poor stability, and smaller potential window. In the

future, the composites of PMDTO with other electrode materials such as carbon, [21] or metal oxides, or new electrolyte system [41] are likely to be a promising way to offset the defects of PMDTO.

5. Conclusions

In this work, a new nitrogen poly(3,4-ethylendioxythiophene) analogue, poly(*N*-methyl-3,4-dihydrothieno[3,4-*b*][1,4]oxazine) modified electrode in supercapacitors was developed via an electrochemical deposition strategy, and the capacitive performance was compared with that of poly(3,4-ethylendioxythiophene). The experimental results show that poly(*N*-methyl-3,4-dihydrothieno[3,4-*b*][1,4]oxazine) has some advantages for supercapacitor (low oxidation potential of the monomer, relatively higher specific capacitance values) and still suffered from the drawbacks of decreased rigidity, poor stability, and smaller potential window.

The scanning electron microscope of the fabricated poly(*N*-methyl-3,4-dihydrothieno[3,4-*b*][1,4]oxazine) electrodes displayed a sponge-like morphology structure, which was characteristic for ideal pseudocapacitive applications. For poly(*N*-methyl-3,4-dihydrothieno[3,4-*b*][1,4]oxazine) electrode, a specific capacitance of as high as 154.3 F g^{-1} was obtained at a current density of 3 A g^{-1} in acetonitrile-tetrabutyl-ammonium tetrafloroborate, while it was 134.6 F·g^{-1} for poly(3,4-ethylendioxythiophene) electrode under the same conditions. Electrochemical results also demonstrated that

poly(*N*-methyl-3,4-dihydrothieno[3,4-*b*][1,4]oxazine) exhibited stability with maximal capacitance retention of nearly 71% after 500 cycles at a current density of 10 A g^{-1}. However, the measurements of the symmetric supercapacitor based on two poly(*N*-methyl-3,4-dihydrothieno[3,4-*b*][1,4]oxazine) electrodes is failure. The asymmetrical supercapacitor based on poly(N-methyl-3,4-dihydrothieno[3,4-b][1,4]oxazine) electrode and poly(3,4-ethylendioxythiophene) electrode exhibited better capacitance performance when compared with the poly(3,4-ethylendioxythiophene) symmetrical supercapacitor.

Further efforts are needed so that poly(*N*-methyl-3,4-dihydrothieno[3,4-*b*][1,4]oxazine) can be used in the field of super capacitors. The composites of poly(*N*-methyl-3,4-dihydrothieno[3,4-*b*][1,4]oxazine) with other electrode materials (carbon, metal oxides, and new electrolyte system) are likely to be a promising way to overcome the drawbacks of poly(*N*-methyl-3,4-dihydrothieno[3,4-*b*][1,4]oxazine).

Acknowledgement

This work was supported by the National Natural Science Foundation of China (grant number: 51303073, 51463008), the Science and Technology Landing Plan of Universities in Jiangxi province (KJLD12081), Jiangxi Provincial Postdoctoral Preferential Foundation (2013KY14), Postdoctoral Starting-up Foundation of Jiangxi Science and Technology Normal University (3000035608) and Postdoctoral Starting-up Foundation of Nanchang City.

References

1 I. F. Perepichka and D. F. Perepichka, *John Wiley & Sons*, Ltd, Chichester, 2009.

2, H. Meng, J. Zheng, A. J. Lovinger, B. Wang, P. G. Van Patten and Z. Bao, *Chem. Mater.*, 2003, **15**, 1778.

3 W. U. Huynh, J.J. Dittmer and A. P. Alivisatos, *Science*, 2002, **295**, 2425.

4 A. Elschner, S. Kirchmeyer, W. Lvenich, U. Merker and K. Reuter, *Taylor & Francis Group*, Boca Raton, 2011.

5 A. Czardybon and M. Lapkowski, *Synth. Met.*, 2001, **119**, 161.

6 S. Chen, B.Y. Lu, X.M. Duan and J.K. Xu, *J Polym. Sci. Pol. Chem.*, 2012, **50**, 1967.

7 D. Aradilla, F. Estrany and C. Alem, *J. Phys. Chem. C,* 2011, **115**, 8430.

8 R. Liu, S.Il. Cho and S.B. Lee, *Nanotechnology*, 2008, **19**, 215710.

9 Y.L. Xu, J. Wang, W. Sun and S.H Wang, *J. Power Sources*, 2006, **159**, 370.

10. R. Liu and S. B. Lee, *J. Am. Chem. Soc*., 2008, **130**, 2942.

11 Sellam and S. A. Hashmi, *ACS Appl. Mater. Interfaces*, 2013, **5**, 3875.

12 W. Chen, C. Xia and H. N. Alshareef, *ACS Nano,* 2014, **9**, 9531.

13 L.L. Zhang and X.S. Zhao, *Chem. Soc. Rev.*, 2009, **38**, 2520.

14 J.L.Liu, L.L. Zhang, H.B. Wu, J.Y. Lin, Z.X. Shen and X.W. Lou, *Energy Environ. Sci.,* 2014, **7**, 3709.

15 J.L. Liu, J. Sun and L. Gao, *J. Phys. Chem. C*., 2010, **114**, 19614.

16 J.L. Liu, J. Sun, L. Gao, Nanoscale., 2011, **3**, 3616.

17A. Rudge, J. Davey and I. Raistrick, *J. Power Sources*, 1994 , **47**, 89.

18 K. Wang, J. Huang and Z.X. Wei, J. *Phys. Chem. C*, 2010, **114**, 8062.

19 G. Inzelt, *Springer Verlag*, Berlin, 2008.

20 G. A. Snook, P. Kao and A. S. Best, *J. Power Sources*,2011, **196**, 1.

21 K. Lota, V. Khomenko and E. Frackowiak, *J. Phys. Chem. Solids,* 2004, **65**, 295.

22 Y.Li, B.C. Wang, H.M. Chen and W. Feng, *J. Power Sources*, 2010, **195**, 3025.

23 K.K.Liu, Z.L. Hu, R. Xue, J.R. Zhang and J.J. Zhu, *J. Power Sources*, 2008, **179**, 858.

24 W.K. Li, J. Chen, J.J. Zhao, J.R. Zhang and J.J. Zhu, *Mater. Lett.*, 2005, **59**, 800.

25 G. P. Pandey, A. C. Rastogi and C. R. Westgate, *J. Power. Sources,* 2014, **245**, 857.

26 B. Babakhani and D.G. Ivey, *Electrochim. Acta,* 2010, **55**, 4014.

27 L. Li, D. C. Loveday, D.S. K. Mudigonda and J.P. Ferraris, *J. Electrochem. Soc.,* 2002, **149**, A1201.

28 J. Tanguy, M. Slama, M. Hoclet and J.L. Baudouin, *Synth. Met.,* 1989, **28**, 145.

29 M. Wilamowska and A. Lisowska-Oleksiak, *J. Power. Sources,* 2009, **194**, 112.

30 M. Güllü and D. Yiğit, *Synth. Met.,* 2012, **162**, 1434.

31 E. Ermis, D. Yiğit and M. Güllü, *Electrochim. Acta,* 2013, **90**, 623.

32 D. Yiğit, T. Güngör and M. Güllü, *Org. Electron.*, 2013, **14**, 3249.

33 D.Y. Liu and J. R. Reynolds, *ACS Appl. Mater. Interfaces,* 2010, **12**, 3586.

34 J. Tang, Z. P. Song, N. Shan, L. Z. Zhan, J. Y. Zhang, H. Zhan, Y. H. Zhou and C. M. Zhan, *J. Power. Sources,* 2008, **185**, 1434.

35 J.K. Xu, G.M. Nie, S.S. Zhang, X.J. Han, J. Hou and S.Z. Pu, *J. Polym. Sci. Part A: Polym. Chem.*, 2005, **43**, 1444.

36 W.Q. Zhou, Y.K. Du, H.M. Zhang, J.K. Xu and P. Yang, *Electrochim. Acta*, 2010, **55**, 2911.

37 W.Q. Zhou, Y.K. Du, F.F. Ren, C.Y. Wang, J.K. Xu and P. Yang, *Int. J. Hydrogen. Energy*, 2010, **35**, 3270.

38 M. J. Frisch; G. W. Trucks; H. B. Schlegel; G. E. Scuseria; M. A. Robb; J. R. Cheeseman; J. A. Montgomery Jr, T. Vreven, K. N. Kudin, J. C. Burant, J. M. Millam, S. S. Iyengar, J. Tomasi, V. Barone, B. Mennucci, M. Cossi, G. Scalmani, N. Rega, G. A. Petersson, H. Nakatsuji, M. Hada, M. Ehara, K. Toyota, R. Fukuda, J. Hasegawa, M. Ishida, T. Nakajima, Y. Honda, O. Kitao, H. Nakai, M. Klene, X. Li, J. E. Knox, H. P. Hratchian, J. B. Cross, C. Adamo, J. Jaramillo, R. Gomperts, R. E. Stratmann, O. Yazyev, A. J. Austin, R. Cammi, C. Pomelli, J. W. Ochterski, P. Y. Ayala, K. Morokuma, G. A. Voth, P. Salvador, J. J. Dannenberg, V. G. Zakrzewski, S. Dapprich, A. D. Daniels, M. C. Strain, O. Farkas, D. K. Malick, A. D. Rabuck, K. Raghavachari, J. B. Foresman, J. V. Ortiz, Q. Cui, A. G. Baboul, S. Clifford, J. Cioslowski, B. B. Stefanov, G. Liu, A. Liashenko, P. Piskorz, I. Komaromi, R. L. Martin, D. J. Fox, T. Keith, M. A. AlLaham, C. Y. Peng, A. Nanayakkara, M. Challacombe, P. M. W. Gill, B. Johnson, W. Chen, M. W. Wong, C. Gonzalez and J. A. Pople, Gaussian 03, Revision C.02, Gaussian, Inc., Wallingford CT, 2004.

39 R. G. Parr and W. Yang, Density-functional Theory of Atoms and Molecules, Oxford University Press, New York, 1989.

40 W. Koch and M. C. Holthausen, A Chemist's Guide to Density Functional Theory,

Wiley-VCH, New York, 2000.

41C. Lee, W. Yang and R. G. Parr, Phys. Rev. B: Condens. Matter Mater. Phys., 1988, 37, 785-789.

42 A. D. Becke, J. Chem. Phys., 1993, 98, 5648-5652.

43 Z.P. Wang, J.K. Xu, B.Y. Lu, S.M. Zhang, L.Q. Qin, D.Z. Mo and S.J. Zhen, *Langmuir* 2014, **30**, 15581.

44 B.Y. Lu, S.M. Zhang, L.Q. Qin, S. Chen, S.J. Zhen and J.K. Xu, *Electrochim. Acta*, 2013, **106**, 201.

45 Z.L. Feng, D.Z. Mo, Z.P. Wang, S.J. Zhen, J.K. Xu, B.Y. Lu, S.L. Ming, K.W. Lin and J.H. Xiong, *Electrochim. Acta*, 2015, **160**, 160.

46 G. Zotti, S. Zecchin, G. Schiavon and L.B. Groenendaal, *Chem. Mater.* 2000, **12**, 2996.

47 H.C. Li, C. Lambert and R. Stahl, *Macromolecules*, 2006, **39**, 2049.

48 P. Schottland, K. Zong, C.L. Gaupp, B.C. Thompson, C.A. Thomas, I. Giurgiu, R. Hickman, K.A. Abboud and J.R. Reynolds, *Macromolecules*, 2000, **33**, 7051.

49 C.A. Thomas, K. Zong, P. Schottland and J.R. Reynolds, *Adv. Mater.*, 2000, **12**, 222.

50 D.Z. Mo, W.Q. Zhou, X.M. Ma and J.K. Xu, *Electrochim. Acta*., 2015, **155**, 29.

51 C.G. Wang, J. L. Schindler, C. R. Kannewurf and M. G. Kanatzidis, *Chem. Mater.*, 1995, **7**, 58.

52 H. Pang, P. J. Skabara, S. Gordeyev, J. J. W. McDouall, S. J. Coles and M. B. Hursthouse, *Chem. Mater.,* 2007, **19**, 301.

53 E. Sahin, E. Sahmetlioglu, I. M. Akhmedov, C. Tanyeli and L. Toppare, Org. Electron., 2006, 7, 351.

54 M. Aka, A. Durmus and L. Toppare, Solid State Sci., 2007, **9**, 843.

55 B. Dong, L.Q. Zheng, J.K. Xu, H.T. Liu and S.Z. Pu, *Polymer*, 2007, **48**, 5548.

56 G.M. Nie, T. Cai, S.S. Zhang, Q. Bao and J.K. Xu, *Electrochim. Acta*, 2007, **52**, 7097.

57 B. Dong, Y.H. Xing, J.K. Xu, L.Q. Zheng, J. Hou and F. Zhao, *Electrochim. Acta*, 2008, **53**, 5745.

58 B.Y. Lu, L.Q. Zeng, J.K. Xu, G.M. Nie and T. Cai, *Acta. Chim. Sinica,* 2008, 66, 1593.

59 W. Domagala, D. Palutkiewicz, D. C. Lacalle, A. L. Kanibolotsky and P. J. Skabara, *Opt. Mater.*, 2011, **33**, 1405.

60 J.L. Liu, M.H. Chen, L.L. Zhang, J. Jiang, J.X. Yan, Y.Z. Huang, J.Y. Lin, H.J. Fan and Z.X. Shen, *Nano Lett.*, 2014, **14**, 7180.

61 D.Z. Mo, W.Q. Zhou, X.M. Ma, J.K. Xu, F.X. Jiang and D.H. Zhu, *Electrochim. Acta* 2015, **151**, 477.

62 B. Senthilkumar, P. Thenamirtham and R.K. Selvan, *Appl. Surf. Sci.*, 2011, **257**, 9063.

63 J. Wang, Y.L. Xu, X. Chen and X.F. Sun, *Compos. Sci. Technol.*, 2007, **67**, 2981.

64 Y.E. Miao, W. Fan, D. Chen and T.X. Liu, *ACS Appl. Mater. Interfaces*, 2013, **5**, 4423.

65 J.W. Park, S.J. Park, O.S. Kwon, C. Le and J. Jang, *Chem. Mater.*, 2014, **26**,

2354.

66 H.C. Li and C. Lambert, *J. Mater. Chem.*, 2005, **15**, 1235.

67 W.Q. Zhou, X.M. Ma, F.X. Jiang, D.H. Zhu, J.K. Xu, B.Y. Lu and C.C. Liu, *Electrochim. Acta*, 2014, **138**, 270.

68 Y.P. Kayinamura, M. Ovadia, D. Zavitz, J.F. Rubinson, *ACS Appl. Mater. Interfaces*, 2010, **2**, 2653.

69 T. Kobayashi, H.Yoneyamal and H. Tamura, *J. Electroanal. Chem*. 1984, **177**, 281.

70 Q. Li, X.F. Lu, H. Xu, Y.X. Tong and G.R. Li, *ACS Appl. Mater. Interfaces*, 2014, **6**, 2726.

71 Z. Fan, J. Yan, T. Wei, L. Zhi, G. Ning, T. Li and F. Wei, *Adv. Funct. Mater.,* 2011, **11**, 2366.

72 D. Guo, Y. Luo, X. Yu and Q. Li, T, *Nano Energy*, 2014, **8**, 174.

73 M. D. Stoller, S. Park, Y. Zhu, J. Na and R. S. Ruoff, *Nano Lett.*, 2008, **8**, 10.

74 P. Sen and A. De, *Electrochim. Acta*, 2010, **55**, 4677.

75 L. Chen, C. Yuan, H. Dou, B. Gao, S. Chen and X. Zhang, *Electrochim. Acta*, 2009, **54**, 2335.

76 A. V. Murugan, A. K. Viswanath, G. Gampet, C. S. Gopinath and K. Vijayamohanan, *Appl. Phys. Lett.*, 2005, **87**, 243511.

77 R. Sharma and L. Zhai, *Electrochim. Acta*, 2009, **54**, 7148.

79C. G. Liu, Z. N. Yu, D. Neff, A. Zhamu, and B. Z. Jang, *Nano Lett.,* 2010, **10**, 4863.

80 H. J. Spencer, P. J. Skabara, M. Giles, I. McCulloch, S. J. Coles and M. B.

Hursthouse, *J. Mater. Chem.*, 2005, **15**, 4783.

Table of Contents Entry

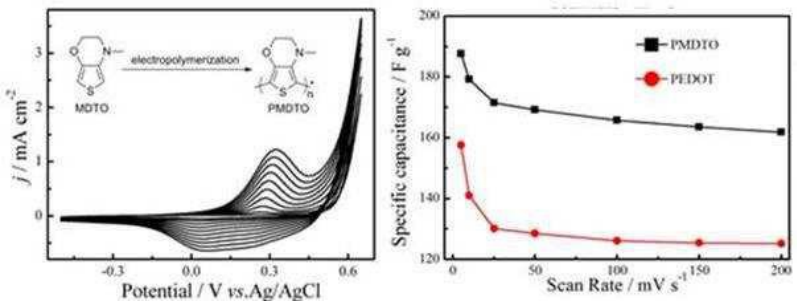

A new nitrogen PEDOT analogue–poly(*N*-methyl-3,4-dihydrothieno[3,4-*b*][1,4]-oxazine) (PMDTO) has some advantages for supercapacitor (low oxidation potential of the monomer, sponge-like morphology structure, and relatively higher specific capacitance values), but still suffered from the drawbacks of decreased rigidity, poor stability, and smaller potential window.